Networks of superconducting nano-puddles in 1/8 doped $YBa_2Cu_3O_{6.5+y}$ controlled by thermal manipulation

2014 New J. Phys. 16 053030

(http://iopscience.iop.org/1367-2630/16/5/053030)

New Journal of Physics
The open access journal at the forefront of physics
Deutsche Physikalische Gesellschaft DPG | IOP Institute of Physics

Networks of superconducting nano-puddles in 1/8 doped $YBa_2Cu_3O_{6.5+y}$ controlled by thermal manipulation

Alessandro Ricci[1,2], Nicola Poccia[2,3], Gaetano Campi[4], Francesco Coneri[3], Luisa Barba[5], Gianmichele Arrighetti[5], Maurizio Polentarutti[5], Manfred Burghammer[6,7], Michael Sprung[1], Martin v Zimmermann[1] and Antonio Bianconi[2,4]

[1] Deutsches Elektronen-Synchrotron DESY, Notkestraße 85, D-22607 Hamburg, Germany
[2] Rome International Center for Materials Science Superstripes RICMASS, via dei Sabelli 119A, I-00185 Roma, Italy
[3] MESA + Institute for Nanotechnology, University of Twente, PO Box 217, 7500AE Enschede, Netherlands
[4] Institute of Crystallography, CNR, via Salaria Km 29.300, Monterotondo Roma, I-00015, Italy
[5] Elettra Sincrotrone Trieste. Strada Statale 14 - km 163, 5, AREA Science Park, I-34149 Basovizza, Trieste, Italy
[6] European Synchrotron Radiation Facility, B. P. 220, F-38043 Grenoble Cedex, France
[7] Department of Analytical Chemistry, Ghent University, Krijgslaan 281, S12 B-9000 Ghent, Belgium
E-mail: phd.alessandro.ricci@gmail.com

Received 11 December 2013, revised 28 February 2014
Accepted for publication 1 April 2014
Published 14 May 2014

New Journal of Physics **16** (2014) 053030
doi:10.1088/1367-2630/16/5/053030

Abstract

While it is known that the nature and the arrangement of defects in complex oxides have an impact on the material functionalities, little is known about control of superconductivity by oxygen interstitial organization in cuprates. Here we report direct compelling evidence for the control of T_c by manipulation of the superconducting granular networks of nanoscale puddles, made of ordered oxygen stripes, in a single crystal of $YBa_2Cu_3O_{6.5+y}$ with average formal hole doping p close to 1/8. Upon thermal treatments we were able to switch from a first network of oxygen defect striped puddles with OVIII modulation ($q_{OVIII}(a^*) = (h + 3/8, k, 0)$ and $q_{OVIII}(a^*) = (h + 5/8, k, 0)$) to a second network characterized by OXVI modulation ($q_{OXVI}(a^*) = (h + 7/16, k, 0)$ and $q$ox-VI

(a*) = (h + 9/16, k, 0)) and finally to a third network with puddles of OV periodicity ($q_{OV}(a^*)$ = (4/10, 1, 0) and $q_{OV}(a^*)$ = (6/10, 1, 0)). We map the microscopic spatial evolution of the out of plane OVIII, OXVI and OV puddle nanosize distribution via scanning micro-diffraction measurements. In particular, we calculated the number of oxygen chains (n) and the charge density (hole concentration p) inside each puddle, analyzing areas of $160 \times 80\ \mu m^2$, and recording 12 800 diffraction patterns to reconstruct each spatial map. The high spatial inhomogeneity shown by all the reconstructed spatial maps reflects the intrinsic granular structure that characterizes cuprates and iron chalcogenides, disclosing the presence of several complex networks of coexisting superconducting domains with different lattice modulations, charge densities and gaps as in the proposed multi-gap scenario called superstripes.

Keywords: phase separation, inhomogeneity, cuprates, high temperature superconductivity, complex materials

1. Introduction

An essential step towards the understanding of modern materials and their implementation in novel nano-electronic devices is the control and manipulation of their microscopic behavior [1–3]. Recently, the interrelationship between spin, charge, and lattice orders in high temperature superconductors (HTSs) has been at the center of a very animated discussion [4–15]. Novel results obtained in $YBa_2Cu_3O_{6+y}$ (YBCO) provide compelling evidence for charge density waves (CDWs), and static magnetic stripes are intertwined and aggregated in nanoscale puddles [16–21]. These domains are spatially separated by superconducting regions composed by ordered lattice stripes [22–26] forming an intrinsically complex lattice of striped puddles called the 'superstripe' scenario [13]. In this scenario the local lattice modulations determine multiple subbands crossing the Fermi level and therefore multi-gap superconductivity below the critical temperature [27, 28]. This theoretical proposal has been recently supported by the prediction of the anomalous isotope coefficient at 1/8 doping [29]. Since the nature and distribution of defects becomes the driving force, their control by thermal annealing is of high relevance. Therefore, a primary task for both fundamental physics and novel nano-electronics is the careful visualization of the effects of a thermal treatment on the system, via imaging the quasi-two-dimensional puddles of oxygen chains in YBCO. Unfortunately, due to the lack of proper local bulk-sensitive probes, the microscopic scenario is still not clear and the real-space and real-time observation of thermally induced rearrangements of superconducting microregions in HTS is a difficult experimental task.

The development of a technique for imaging the nanoscale intrinsic inhomogeneity of oxygen chain organization is the first step to open new opportunities for their manipulation. Here we explore the nanoscale granular patterns arising in a $YBa_2Cu_3O_{6.67}$ single crystal with doping close to 1/8 hole content per Cu site in the $Y(CuO_2)_2$ bilayer. The $YBa_2Cu_3O_{6.67}$ crystal is an ideal system for investigation of inhomogeneity due to the short range ordering of oxygen ions [30] at 1/8 doping. Indeed, it exhibits an incommensurate superlattice of (OVIII) chains indicated by the lattice superstructure modulation at $q_{OVIII}(a^*) = (h + 3/8,\ k,\ 0)$ and $q_{OVIII}(a^*) = (h + 5/8,\ k,\ 0)$. Although the oxygen tendency to form O–Cu–O fragments in the

basal plane has been widely investigated [31, 32], to date there is little information on the spatial distribution of these fragments, and on their inclination towards aggregation in domains.

In the first part of our paper we report the temperature evolution in $YBa_2Cu_3O_{6.67}$ using standard synchrotron x-ray diffraction of the OVIII puddles of oxygen chains. Using the heat treatment we show the formation of a second network of puddles characterized by OXVI superstructure modulation at $q_{OXVI}(a^*) = (h + 7/16,\ k,\ 0)$ and $q_{OXVI}(a^*) = (h + 9/16,\ k,\ 0)$, and finally a third network of OV puddles characterized by the superstructure wavevectors $q_{OV}(a^*) = (4/10,\ 1,\ 0)$ and $q_{OV}(a^*) = (6/10,\ 1,\ 0)$. The measurements provide us with information about the average order of oxygen chains in the sample. In the following, we investigate the dynamics and spatial distribution of OVIII, OXVI and OV domains upon thermal cycling via micro-x-ray diffraction (μXRD). By scanning microscopic areas, this technique provides mixed information of the reciprocal and real-space the bulk structure inhomogeneities, and it has never been applied on a $YBa_2Cu_3O_{6.67}$ single crystal before. Finally, we show how through thermal treatment it is possible to control the puddle size distribution, the number of oxygen chains and their charge density. Indeed using the novel experimental method μXRD it has been possible to directly visualize how the thermal treatment affects the intrinsic nanoscale phase heterogeneity in this cuprate superconductor. We relate these changes to the onset variation of the superconducting temperature, that we readily can control over a range of 2 K.

2. Materials and methods

Starting reagents with ultra-high purity (CuO and Y_2O_3 99.999%, $BaCO_3$ 99.997%) have been employed to grow extremely good single crystals of $YBa_2Cu_3O_{6.67}$ in barium zirconate crucibles by the self-flux technique [33]. Inductively coupled plasma mass spectroscopy indicates a purity of the crystals higher than 99.99 at.%. The oxygen content of the crystal was set to 6.67 by annealing in flowing oxygen at 914 °C, followed by quenching to room temperature under flowing nitrogen gas. The macroscopic oxygen content inhomogeneity was removed by annealing the crystal at 570 °C in a sealed quartz capsule, followed by quenching in an ice–water bath. The crystal was then kept at room temperature to let the short range oxygen order establish. Average structure characterization shows a unit cell described by a $P4/m$ spatial symmetry and lattice dimensions $a = 3.807(11)$ Å, $b = 3.864(12)$ Å and $c = 11.52(2)$ Å, with a unit cell volume of 169.5(8) Å^3.

Temperature dependent x-ray diffraction measurements were made on the XRD1 beamline at the ELETTRA synchrotron storage ring, Trieste. The beamline is placed on a multipole wiggler insertion device operating under the current ELETTRA conditions of 2 GeV ring energy and 400 mA injection current (see figure S1). The samples were oriented on a kappa diffractometer equipped with a motorized goniometric X–Y stage head and a Mar-Research 165 mm CCD camera as detector. The data were collected in transmission mode with a photon energy of 20 keV ($\lambda = 0.619\,92$ Å), selected from the source by a double-crystal Si(111) monochromator and using a beam of $200 \times 200\ \mu m^2$. The 2D CCD detector (MAR-Research) was placed at a distance of 70 mm from the sample. Data from a LaB_6 standard were collected for calibration. Measurements were conducted between 300 and 400 K with a temperature step of 2 K for both the heating (300–400 K) and the cooling (400–300 K) cycles. Temperature was varied and controlled by means of a 700 series Oxford Cryosystems cryo-cooler that allows

working in a range of 90–400 K, guaranteeing accuracy better than ±1 K. All the images measured by single-crystal x-ray diffraction were processed using the FIT2D program jointly with a MATLAB® based software package developed in house. Second, the microscopic behavior of the sample under the thermal treatments has been investigated using scanning μXRD in reflection geometry (in the a–c plane).

The ID13 beamline of the European Synchrotron Radiation Facility (ESRF) is specialized in the delivery of micro-focused x-ray beams for x-ray diffraction experiments. The photon source, in the range 12–13 keV, is an 18 mm period in-vacuum undulator at the ESRF 6.03 GeV storage ring operated in multi-bunch mode with a current of 200 mA. The optics of the micro-focus beamline include compound refractive lenses, Kirkpatrick Baez (KB) mirrors, crossed Fresnel zone plates or waveguides. The ellipsoidal mirror is the main focusing element, demagnifying the source by a factor of 10 (about 40 μm in diameter). The focused beam is defined by a pinhole of 5 μm diameter. The beam is focused by a tapered glass capillary to 1 μm in diameter. The beamline uses two monochromators positioned in series: the first is a liquid N_2 cooled Si-111 double crystal or Si-111 (bounce); the second is a channel cut monochromator employing a single liquid nitrogen cooled Si crystal. The detector of x-ray diffraction images is a high resolution CCD camera (Mar CCD) with point spread function 0.1 mm, 130 mm entrance window and 16 bit readout placed at a distance of about 90 mm from the sample. To scan the sample area it has been moved using two piezoelectric stages in x–y directions and data have been collected in the θ–2θ reflection geometry (see figure S2). The huge number of diffraction patterns collected by μXRD (more than 12 800 for each map) have been processed using a MATLAB® based software package developed in house.

The magnetic behavior versus temperature of our YBCO sample at 1/8 has been characterized by means of the vibrating sample magnetometer (VSM) option in a Physical Property Measurement System (PPMS 6000) from Quantum Design. Here a linear motor vibrates the sample with a frequency of 40 Hz and amplitude of 2 mm at the center of a pick-up coil, and the induced voltage is measured synchronically with the oscillation. A magnetization measurement has been chosen to consist of the averaged value over 40 data points, that is, over a period of 1 s of oscillation. These parameters guarantee a good signal to noise ratio.

3. Results and discussion

The ordering process of the oxygen ions in chain domains has been studied using transmission XRD. The diffraction pattern due to the superlattice reflections was recorded at room temperature and is shown in figure 1(a).

It is possible to distinguish superlattice peaks due to the OVIII (6/16, 1, 0) and (10/16, 1, 0) reflections in the a^*–b^* plane at 300 K, in agreement with previous data [21], which confirms the high quality of our single crystal. We monitored the x-ray diffraction patterns during a thermal cycle from 300 to 400 K, and then back to 300 K, using a slow rate of 0.5 K min^{-1}. The continuous evolution of the superlattice profiles from OVIII to OV through OXVI modulation is shown in figure 1(b). The OVIII (6/16, 1, 0) and (10/16, 1, 0) reflections in the a^*–b^* plane at 300 K evolve into the OXVI (7/16, 1, 0) and (9/16, 1, 0) modulation upon heating to 400 K.

During the subsequent cool-down to 300 K the original OVIII modulation is not restored and a new OXVI phase, identified by the superlattice peaks (7/16, 1, 0) and (9/16, 1, 0), sets in. In figures 1(b)–(e) we report respectively the temperature dependence of the superlattice peak

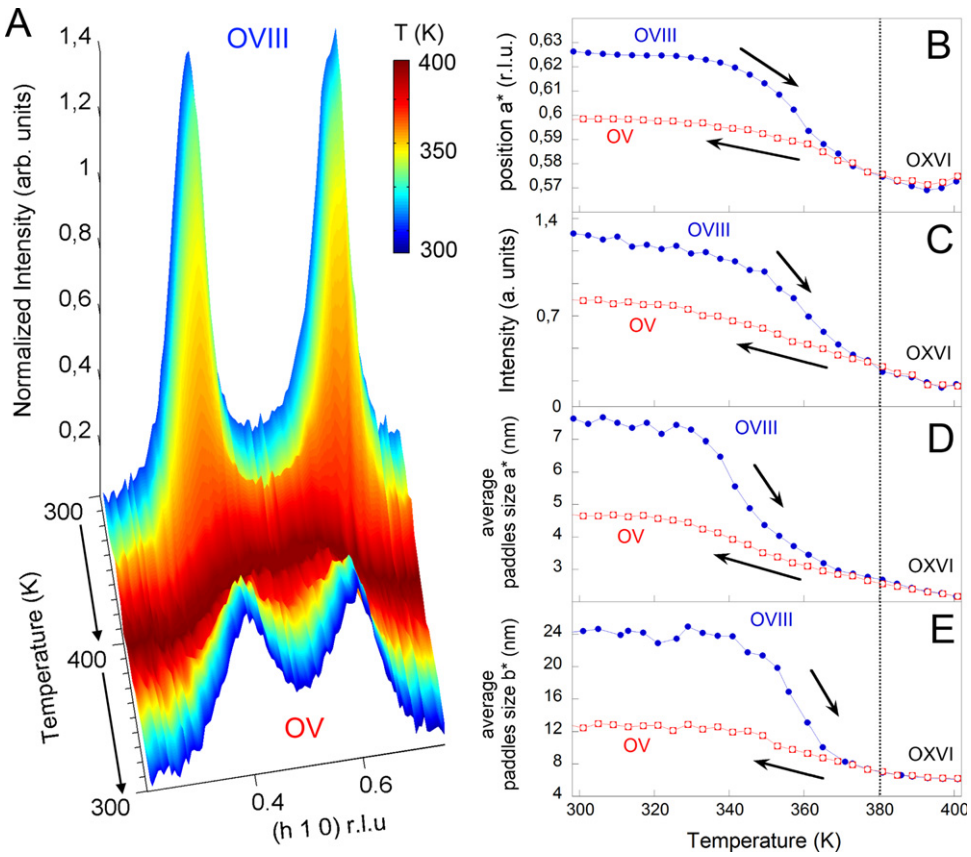

Figure 1. (a) Three dimensional color plot of the thermal evolution of the OVIII oxygen stripe superlattice profile at wavevectors $q_{\mathrm{OVIII}}(a^*) = (3/8, 1, 0)$ and $q_{\mathrm{OVIII}}(a^*) = (5/8, 1, 0)$ into the OV superstructure at wavevector $q_{\mathrm{OV}}(a^*) = (4/10, 1, 0)$ and $q_{\mathrm{OV}}(a^*) = (6/10, 1, 0)$. The temperature ranges from 300 to 400 K, which respectively correspond to dark blue and red colors. The reflections of the superstructures in the $YBa_2Cu_3O_{6+y}$ crystal are measured using a large ($200 \times 200\ \mu m^2$) beam at the ELETTRA storage ring. (b) The thermal cycle of the superlattice position along the a^* crystallographic direction, (c) the intensity, (d) the average puddle size along a^* and (e) along b^*. The arrows show the temporal direction of the experiment. The blue filled circles show the evolution from room temperature to 400 K. The red empty squares show the evolution from 400 K to room temperature. The black dotted line indicates the temperature of 380 K, once crossed the OVIII order can be recovered only by waiting a few days at room temperature.

position, the intensity and the average domain size along a^* and b^*. The average domain size along the in-plane a^* and b^* directions has been calculated by fitting the superlattice reflections with a two-Lorentzian model. In addition, above 380 K the system crosses a OXVI phase with wavevector $q_{\mathrm{mix}} = (h \pm 9/16, k, 0)$. The average size of the OVIII domain along a^* is about 7.5 (5) nm, but approaching the OV it decreases to 4.5(5) nm. The average size is larger along b^*, showing OVIII and OV domains of about 23.5(5) and 11.5(5) nm, respectively. This phenomenology shows that the in plane average domain size of oxygen chains can be controlled and manipulated by tuning the temperature in a quasi-irreversible manner. Leaving the sample under vacuum at room temperature, more than one month is needed for the OV phase to spontaneously drive itself back to a new reconstructed OVIII phase.

This aspect shows relevant analogies with the oxygens and local lattice distortions ordering in La_2CuO_{4+y}, where the Q2-iO phase (due to interstitial oxygen ordering) and the Q3-LLT (due to local lattice distortion ordering) can be changed by thermal treatments and restored by waiting a long time or by the use of x-ray continuous illumination [34–39].

In order to monitor the microscopic evolution of OVIII domains into OXVI and OV during the thermal manipulation, we used μXRD as already successfully done to investigate phase separation appearing in other cuprates [34–39] and iron-based superconductors [40–43]. We made our measurements using a beam about 1 μm in diameter. The sample has been scanned over an area of $160 \times 80\ \mu m^2$ collecting 12 800 micro-diffraction patterns showing superlattices at $q_{OVIII}(a^*) = (3/8, 0, 4)$ and $q_{OVIII}(a^*) = (5/8, 0, 4)$ due to OVIII puddles of ordered oxygen chains. The superlattice peak profiles have been fitted using a two-Lorentzian model, and the satellite position h_{XY} along a^* and the $FWHM_{XY}$ along a^* and c^* have been extracted for every micro-diffraction pattern at the X–Y position.

From the $FWHM_{XY}$ along c^* we calculated the out of plane domain size for every spot of the scanned map. Figures 2(a)–(c) show the real space map of the out of plane domain size (along c^*), before the heating (OVIII), at 390 K (OXVI) and after the cooling cycle (OV), respectively. These maps show the presence of clear intrinsic nanoscale heterogeneity in this cuprate superconductor, as has been observed in iron chalcogenides [40, 42].

The OVIII probability density functions for the domain size distribution along c^* is relatively sharp, and varies from 7 to 9 nm. Upon heating, the OXVI phase shows instead a very broad distribution, that spans the 1–6 nm range. After the cooling cycle, the size distribution in the OV phase sharpens again, around the decreased average value of 3 nm, therefore indicating a certain recovered order. The overall behavior indicates a sensible response of the granular network to thermal treatment.

Starting from the $FWHM_{XY}$ and the h_{XY} along a^*, measured at each X–Y spatial position, we reconstructed the spatial maps of the number of oxygen chains (n) inside the puddles. Using the expression $n_{XY} = (1 - h_{XY})/FWHM_{XY}$, we calculate this quantity for OVIII (figure 3(a)), OXVI (figure 3(b)) and the annealed OV puddles (figure 3(c)).

The number of oxygen chains decreases after the thermal heating cycle from OVIII to OXVI and increases again after the cooling in the OV puddles (but remains lower than in the OVIII phase).

Figures 4(a)–(c) show the spatial map of the charge density (or hole concentration p) inside the puddles of oxygen chains, onto the same area as described in figure 3, before heating (OVIII phase), at 390 K (OXVI phase) and after cool-down (OV phase). The charge density has been calculated considering the difference of the superlattice position along a^* (h_{XY}) with respect to the ortho-II (OII) phase following the relationship $p_{XY} = h_{XY} - 0.5$, where the OII modulation corresponds to a periodicity of a filled CuO chain intercalated by one empty chain. During the thermal annealing process the charge density changed on the microscopic scale and its distribution in the OXVI and OV puddles gets broader, demonstrating the strong granularity of the system. Figure 5(a) shows the spot to spot charge density (p_{XY}) as a function of the number of oxygen chains (n_{XY}), inside the OVIII, OXVI and OV puddles. The behavior has been fitted using an exponential model: $p_{XY} = 1 - \exp\{-[(n_{XY} - n_0)/n_0]\}/\xi_n$. Here n_0 and ξ_n are the minimum and the maximum number of chains present in the average puddle. In order to understand how the microscopic reduction of the effective hole doping affects the superconducting properties, we studied the magnetic response of our sample across the superconducting transition before

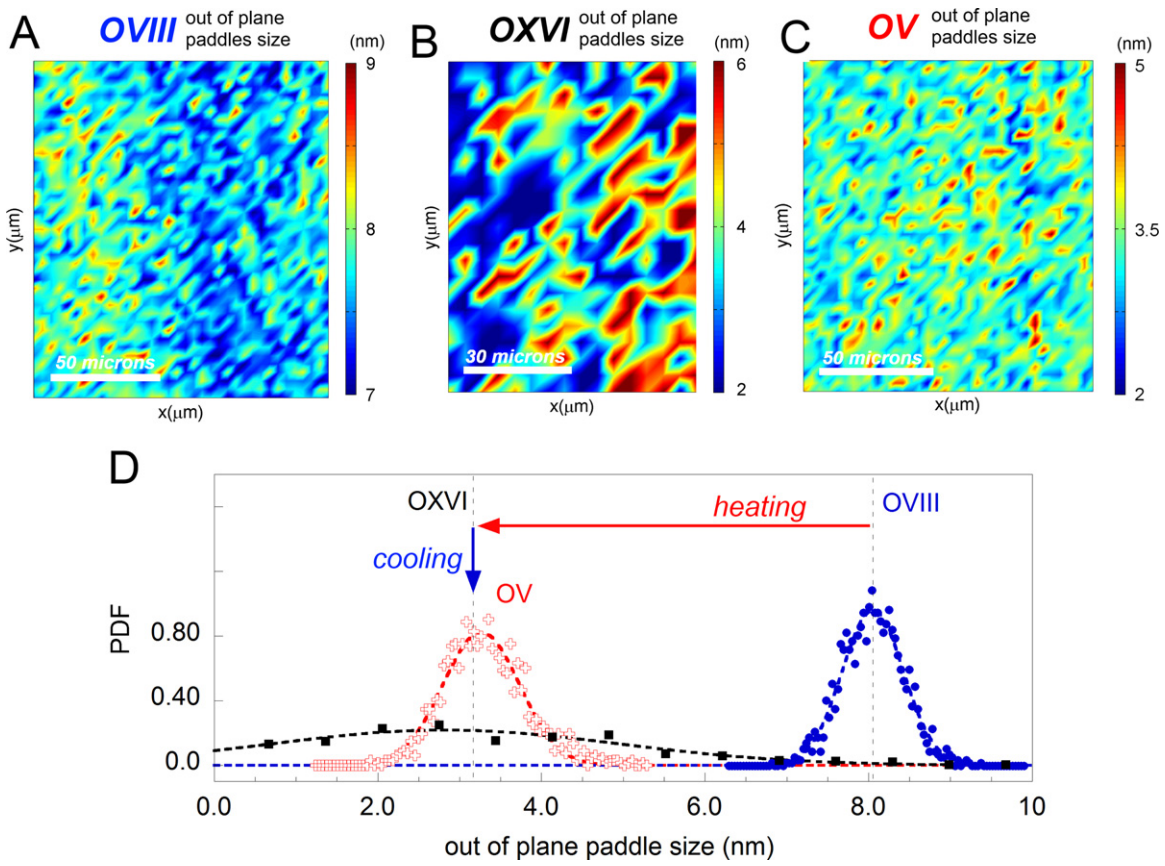

Figure 2. The out of plane puddle sizes (puddle sizes along c^*) before the heating cycle (a), at 390 K (b) and at the end of the cooling cycle (c) in the OVIII, OXVI and OV phases, respectively. (d) The probability density function of the OVIII (blue filled circles), OXVI (black filled squares) and OV (red empty crosses) out of plane puddle sizes. The out of plane puddle sizes decrease after the thermal heating cycle from OVIII to OXVI, where their distribution looks very broad. After the cooling cycle the average out of plane puddle sizes remain the same in the OV phase. On the other hand, the shape of the distribution becomes much sharper, indicating a certain recovered order. Dotted lines are guides for the eyes.

and after the thermal annealing, i.e. in the OVIII and in the OV phase, by means of the VSM option in a PPMS 6000 from Quantum Design. The results are shown in figure 5(b). A first measurement is made before any annealing procedure is carried out (OVIII phase), and shows the onset temperature of the diamagnetic screening (T_c) to be about 66 K. The subsequent measurements are made upon thermal annealing at 380 K (OV phase), with increasing dwell time of 30, 60, 90 and 150 min. In all these cases T_c decreases by about 2 K. This effect is irrespective of the annealing time, and we associate such a reduction with the lower effective charge density we point out in figures 4 and 5(a).

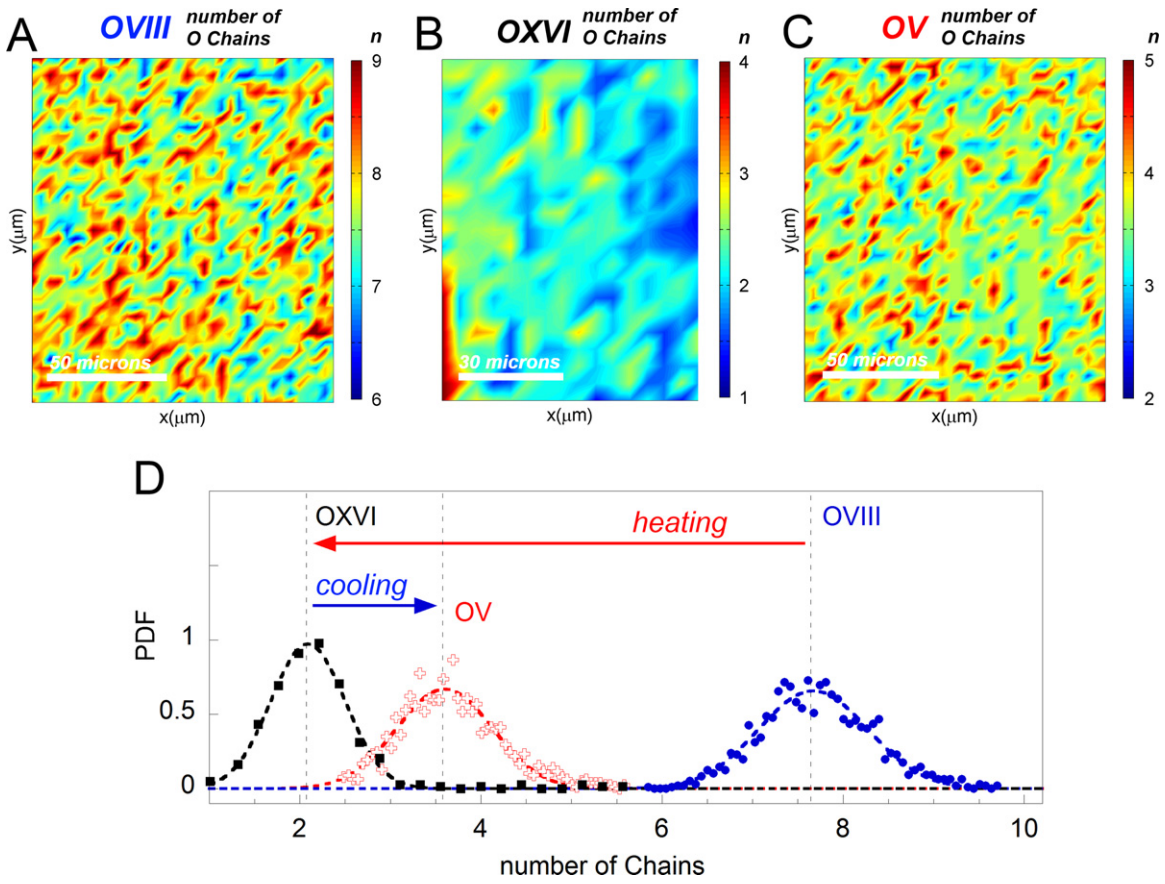

Figure 3. (a)–(c) The spatial map of the number of oxygen chains inside the OVIII, OXVI and OV puddles. (d) Distribution of the number of oxygen chains in the OVIII (blue filled circles), OXVI (black filled squares) and OV (red empty crosses) puddles. The number of oxygen chains decreased after the thermal heating cycle from OVIII to OXVI and increased again after cooling in the OV puddles, but remains lower than in the OVIII phase. Dotted lines are guides for the eyes.

4. Conclusion

In conclusion, we have investigated how thermal treatments allow us to microscopically manipulate and control the functional properties of $YBa_2Cu_3O_{6.67}$ ($p \approx 1/8$). We used an x-ray diffraction approach, combining standard synchrotron XRD measurements ($200 \times 200\,\mu m^2$ beam size) with scanning μXRD ($1 \times 1\,\mu m^2$) and VSM. Using thermal annealing we induced a continuous phase transition that led to a different final arrangement of Cu–O chains in the sample. In particular we monitored a transition from the OVIII to the OV modulation for the oxygen chain domains, by cycling between 300 and 400 K. The microscopic dynamics of the domains have been investigated by scanning μXRD. We mapped with micrometric resolution the out of plane domain size, the number of oxygen chains and the charge density inside each domain, covering a total area of $160 \times 80\,\mu m^2$. We recorded 12 800 diffraction patterns for each spatial map, showing a high nanoscale inhomogeneity and the presence of a complex network-like organization of competing superconducting puddles that are characterized by different numbers of oxygen chains and charge densities. Reductions in the out of plane domain size, in

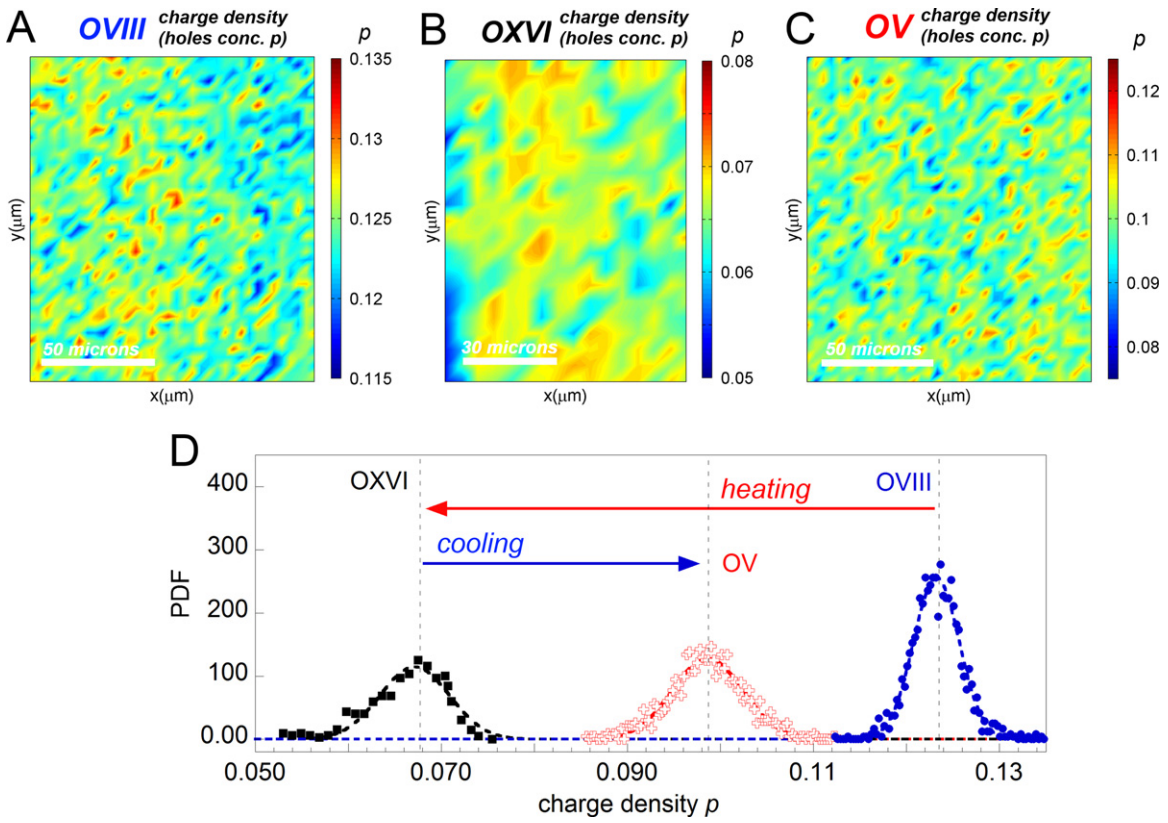

Figure 4. (a)–(c) The spatial map of the charge density (hole concentration p) of the OVIII, OXVI and OV puddles. (d) Distribution of the charge density in the OVIII (blue filled circles), OXVI (black filled squares) and OV (red empty crosses) puddles. During the thermal annealing process the charge density changes and its distribution in the OXVI and OV puddles gets broader.

the number of oxygen chains and in the microscopic distribution of charge density have been observed in the OV phase. These reductions have been connected to a decrease of the number of holes in the active layer. As a consequence, magnetization measurements show that the modification of the network structure of superconducting grains is responsible for a drop of T_c of about 2 K. This can open the way to a possible T_c tuning by microscopic thermal manipulation of the oxygen chain distribution in HTSs. This work shows the presence of a microscale phase separation in $YBa_2Cu_3O_{6.67}$ with a hole doping close to 1/8, where the lattice misfit strain [43] in these heterostructures at atomic limit and the proximity of the Fermi level to a 2.5 Lifshitz transition near a band edge of the subbands [44, 45, 27–29] induce the observed nanoscale phase separation predicted by the multiband Hubbard model [46]. Finally, in this experiment we observe a superstripe [13] lattice scenario in $YBa_2Cu_3O_{6.67}$ made of different striped nanoscale puddles of locally ordered interstitials with well defined hole doping density. The unique information that our experiment provides on the density distribution of the nanoscale striped puddles shows complex networks of superconducting units, that supports the statistical physics theories of percolative superconductivity in complex networks as an essential feature for understanding the emerging high temperature superconductivity [47–51]. In fact, the reconstructed spatial maps shown here provide compelling evidence for the generic granular

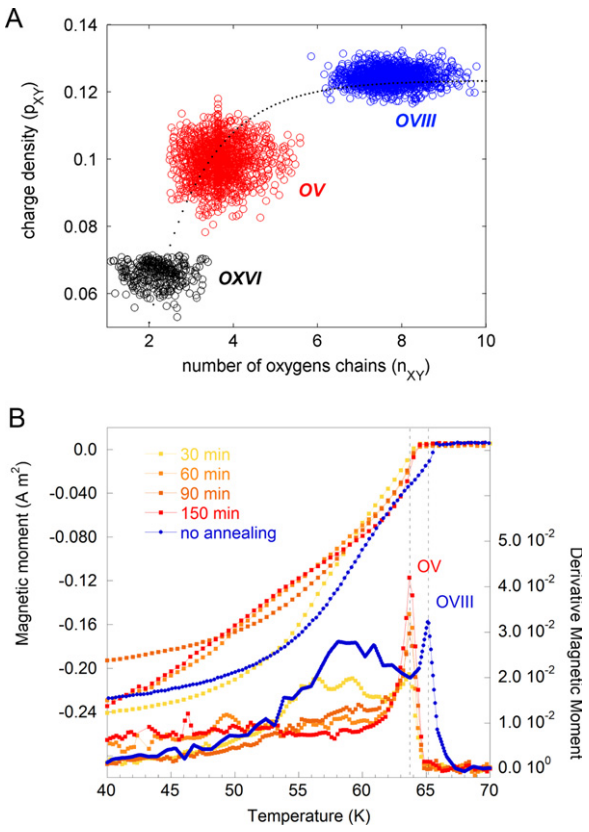

Figure 5. (a) Charge density (hole concentration p) as a function of the number of oxygen chains, inside the OVIII, OXVI and OV puddles. The dotted curve is a fit using a model: $p = 1 - \exp\{-[(n - n_0)/n_0]\}/\xi_n$, where n_0 and ξ_n are the minimum and the maximum number of chains present in the average puddle. (b) Left scale: zero field cooling (ZFC) diamagnetic response of YBCO upon thermal cycles in an external applied field $H = 20$ Oe. Blue filled circles: signal before any thermal annealing. Yellow–red squares: the magnetic moment upon sample annealing at 380 K with increasing dwell time of 30, 60, 90 and 150 min. Right scale: numerical derivative of the magnetic moment. Upon thermal cycling the onset of superconducting shielding decreases by about 2 K.

structure that characterizes cuprates and iron chalcogenides. We disclose practical multiple realizations of complex networks of dopant self-organization at the nanoscale with striped puddles characterized by different modulations, local charge densities and superconducting condensates, which share the common features for the emergence of high T_c superconductivity.

Acknowledgments

We thank Ruixing Liang, D A Bonn, and Walter N Hardy of the Department of Physics of the University of British Columbia for providing us with the crystals and for helpful discussions. We thank the ID13 beamline staff of ESRF and the XRD1 beamline staff of ELETTRA, especially G Bais N P acknowledges the Marie Curie Intra-European Fellowship for financial support.

References

[1] Hwang H Y, Iwasa Y, Kawasaki M, Keimer B, Nagaosa N and Tokura Y 2012 Emergent phenomena at oxide interfaces *Nat. Mater.* **11** 103–13

[2] Huijben M, Brinkman A, Koster G, Rijnders G, Hilgenkamp H and Blank D H A 2009 Structure–property relation of SrTiO3/LaAlO3 interfaces *Adv. Mater.* **21** 1665–77

[3] Mannhart J and Schlom D G 2010 Oxide interfaces—an opportunity for electronics *Science* **327** 1607–11

[4] Dagotto E 2005 Complexity in strongly correlated electronic systems *Science* **309** 257–62

[5] Littlewood P 2011 Superconductivity: an x-ray oxygen regulator *Nat. Mater.* **10** 726–7

[6] Zaanen J 2010 High-temperature superconductivity: the benefit of fractal dirt *Nature* **466** 825–7

[7] Zeljkovic L and Hoffman J E 2013 Interplay of chemical disorder and electronic inhomogeneity in unconventional superconductors *Phys. Chem. Chem. Phys.* **15** 13462

[8] Bishop A R, Shenoy S R and Sridhar S (ed) 2003 *Intrinsic Multiscale Structure and Dynamics in Complex Electronic Oxides* (New Jersey: Word Scientific)

[9] Kalinin S V and Spaldin N A 2013 Functional ion defects in transition metal oxides *Science* **341** 858–9

[10] Borisenko S 2013 Superconductivity: fewer atoms, more information *Nat. Mater.* **12** 600–1

[11] Saini N L 2013 Nanoscale structure and atomic disorder in the iron-based chalcogenides *Sci. Technol. Adv. Mater.* **14** 014401

[12] Giraldo-Gallo P *et al* 2013 Inhomogeneous superconductivity in $BaPb_{1-x}Bi_xO_3$ *J. Supercond. Novel Magn.* **26** 2575

[13] Bianconi A S 2000 Superstripes *Int. J. Mod. Phys.* B **14** 3289–97

[14] Christensen R B, Hirschfeld P J and Andersen B M 2011 Two routes to magnetic order by disorder in underdoped cuprates *Phys. Rev.* B **84** 184511

[15] Phillips J C 2014 Ineluctable complexity of high temperature superconductivity elucidated *J. Supercond. Novel Magn.* **27** 345–7

[16] Tranquada J M 2012 Cuprates get orders to charge *Science* **337** 811–2

[17] Hücker M *et al* 2013 Enhanced charge stripe order of superconducting $La_{2-x}Ba_xCuO_4$ in a magnetic field *Phys. Rev.* B **87** 014501

[18] Hücker M 2012 Structural aspects of materials with static stripe order *Physica C* **481** 3–14

[19] Wu T *et al* 2011 Magnetic-field-induced charge-stripe order in the high-temperature superconductor $YBa_2Cu_3O_y$ *Nature* **477** 191–4

[20] Chang J *et al* 2012 Direct observation of competition between superconductivity and charge density wave order in $YBa_2Cu_3O_{6.67}$ *Nat. Phys.* **8** 871–6

[21] Ghiringhelli G *et al* 2012 Long-Range incommensurate charge fluctuations in $(Y,Nd)Ba_2Cu_3O_{6+x}$ *Science* **337** 821–5

[22] Achkar A J *et al* 2012 Distinct charge orders in the planes and chains of ortho-iii-ordered $YBa_2Cu_3O_{6+\delta}$ superconductors identified by resonant elastic x-ray scattering *Phys. Rev. Lett.* **109** 167001

[23] Bianco-Canosa S *et al* 2013 Momentum-dependent charge correlations in $YBa_2Cu_3O_{6+y}$ superconductors probed by resonant x-ray scattering: evidence for three competing phases *Phys. Rev. Lett.* **110** 187001

[24] Campi G *et al* 2013 Scanning micro-x-ray diffraction unveils the distribution of oxygen chain nanoscale puddles in $YBa_2Cu_3O_{6.33}$ *Phys. Rev.* B **87** 014517

[25] Ricci A *et al* 2013 Multiscale distribution of oxygen puddles in 1/8 doped $YBa_2Cu_3O_{6.67}$ *Sci. Rep.* **3** 2383

[26] Bianconi A 2013 Quantum materials: shape resonances in superstripes *Nat. Phys.* **9** 536–7

[27] Bianconi A *et al* 1996 Stripe structure in the CuO_2 plane of perovskite superconductors *Phys. Rev.* B **54** 12018

[28] Perali A *et al* 1996 The gap amplification at a shape resonance in a superlattice of quantum stripes: A mechanism for high T_c *Solid State Commun.* **100** 181

[29] Perali A *et al* 2012 Anomalous isotope effect near a 2.5 Lifshitz transition in a multi-band multi-condensate superconductor made of a superlattice of stripes *Superconducting Sci. Technol.* **25** 124002

[30] Zimmermann V *et al* 2003 Oxygen-ordering superstructures in underdoped $YBa_2Cu_3O_{6+x}$ studied by hard x-ray diffraction *Phys. Rev.* B **68** 104515
[31] Jorgensen J D *et al* 1987 Oxygen ordering and the orthorhombic-to-tetragonal phase transition in $YBa_2Cu_3O_{7-x}$ *Phys. Rev.* B **36** 3608
[32] Jorgensen J D *et al* 1990 Structural properties of oxygen-deficient $YBa_2Cu_3O_{7-\delta}$ *Phys. Rev.* B **41** 1863
[33] Liang R, Bonn D A and Hardy W N 2012 Growth of YBCO single crystals by the self-flux technique *Phil. Mag.* **92** 2356
[34] Bianconi A, Di Castro D, Bianconi G, Pifferi A, Saini N L, Chou F C *et al* 2000 Coexistence of stripes and superconductivity: T_c amplification in a superlattice of superconducting stripes *Physica C* **341** 1719–22
[35] Poccia N *et al* 2011 Evolution and control of oxygen order in a cuprate superconductor *Nat. Mater.* **10** 733–6
[36] Poccia N, Bianconi A, Campi G, Fratini M and Ricci A 2012 Size evolution of the oxygen interstitial nanowires in La_2CuO_{4+y} by thermal treatments and x-ray continuous illumination *Superconductor Sci. Technol.* **25** 124004
[37] Fratini M *et al* 2010 Scale-free structural organization of oxygen interstitials in La_2CuO_{4+y} *Nature* **466** 841–4
[38] Poccia N *et al* 2012 Optimum inhomogeneity of local lattice distortions in La_2CuO_{4+y} *Proc. Natl Acad. Sci.* **109** 15685–90
[39] Poccia N *et al* 2011 Spatial inhomogeneity and planar symmetry breaking of the lattice incommensurate supermodulation in the high-temperature superconductor $Bi_2Sr_2CaCu_2O_{8+y}$ *Phys. Rev.* B **84** 100504
[40] Ricci A *et al* 2011 Nanoscale phase separation in the iron chalcogenide superconductor $K_{0.8}Fe_{1.6}Se_2$ as seen via scanning nanofocused x-ray diffraction *Phys. Rev.* B **84** 060511
[41] Fratini M, Caivano R, Puri A *et al* 2008 The effect of internal pressure on the tetragonal to monoclinic structural phase transition in ReOFeAs: the case of NdOFeAs *Superconductor Sci. Technol.* **21** 092002
[42] Ricci A, Poccia N, Joseph B *et al* 2011 Intrinsic phase separation in superconducting $K_{0.8}Fe_{1.6}Se_2$ ($T_c = 31.8$ K) single crystals *Superconductor Sci. Techn.* **24** 082002
[43] Poccia N, Ricci A and Bianconi A 2010 Misfit strain in superlattices controlling the electron-lattice interaction via microstrain in active layers *Adv. Condens. Matter Phys.* **2010** 261849
[44] Bianconi A, Valletta A, Perali A *et al* 1997 High T_c superconductivity in a superlattice of quantum stripes *Sol. State Commun.* **102** 369–74
[45] Romero-Bermúdez A and García-García A M 2014 Shape resonances and shell effects in thin-film multiband superconductors *Phys. Rev.* B **89** 024510
[46] Kugel K I *et al* 2008 Model for phase separation controlled by doping and the internal chemical pressure in different cuprate superconductors *Phys. Rev.* B **78** 165124
[47] de Mello E V L 2012 Describing how the superconducting transition in La_2CuO_{4+y} is related to the iO phase separation *J. Supercond. Novel Magn.* **25** 1347–50
[48] Bianconi G 2012 Superconductor-insulator transition on annealed complex networks *Phys. Rev.* E **85** 061113
[49] Bianconi G E P L 2013 Superconductor-insulator transition in a network of 2d percolation clusters *Europhys. Lett.* **101** 26003
[50] Gor'kov L P and Teitel'baum G B 2008 The two-component physics in cuprates in the real space and in the momentum representation *J. Phys.: Conf. Ser.* **108** 012009
[51] Yukalov V I and Yukalova E P 2014 Statistical theory of materials with nanoscale phase separation *J. Supercond. Novel Magn.* **27** 919–24